Neutron Emission Rate Characteristics of an Electron Cyclotron Heated Large Helical Device Deuterium Plasma*)

Kunihiro OGAWA[1,2], Mitsutaka ISOBE[1,2], Ryosuke SEKI[1,2], Hideo NUGA[1], Siriyaporn SANGAROON[1,3], Jungmin JO[4] and Masaki OSAKABE[1,2]

[1]*National Institute for Fusion Science, National Institutes of Natural Sciences, Toki 509-5292, Japan*
[2]*The Graduate University for Advanced Studies, SOKENDAI, Toki 509-5292, Japan*
[3]*Faculty of Science, Mahasarakham University, Maha Sarakham 44150, Thailand*
[4]*Korea Institute of Fusion Energy, Daejeon 34133, Republic of Korea*

(Received 27 October 2020 / Accepted 21 December 2020)

The total neutron emission rate (S_n) characteristics of electron cyclotron heated plasma were surveyed in the Large Helical Device in order to exhibit the thermonuclear performance of helical plasma. The dependence of S_n on electron density showed that S_n increased with an electron density of power of 3.1. To understand S_n, characteristics in the electron cyclotron heated plasma, a numerical simulation considering thermal deuterium-deuterium fusion reactions was performed. Although the numerical simulation overestimated S_n in a relatively low S_n region, calculated S_n matched the experimental result for a relatively high S_n region. A possible reason for the disagreement in the low S_n region is that effective charge due to the impurities such as carbon is changed because of the low density.

Keywords: Large Helical Device, thermal plasma, total neutron emission rate, neutron flux monitor, electron cyclotron heating

DOI: 10.1585/pfr.16.2402008

1. Introduction

In a fusion reactor, deuterium-tritium (DT) reaction occurs continuously in high-temperature plasma. The alpha particles created by this DT reaction are used for the self-heating of plasma, whereas the kinetic energy of DT born neutron absorbed by the blanket module will be used for power generation. As such, neutron emission is a direct value of the progress toward achieving the requirements of a thermonuclear reactor. For example, in large tokamaks, break-even or nearly break-even plasma conditions were achieved using intensive neutral beam injections for a short time [1–3]. Conversely, by 2017, deuterium plasma experiments in large-sized stellarators and helical devices had not yet been conducted. In the Large Helical Device (LHD), a deuterium plasma experiment was initiated in March 2017 that is considered the first deuterium experiment in large-sized stellarators/helical devices [4–6]. One of the aims of this experiment is to illustrate the performance of helical plasma toward a fusion reactor. After initiating deuterium plasma experiments in an LHD, fusion performance toward a helical reactor, e.g., a total neutron emission rate (S_n) of 3.3×10^{15} n/s and an equivalent DT fusion gain of 0.11, was achieved using intensive neutral beam injections [7, 8]. Although this progress is significant, these accomplishments were achieved in neutral beam heated plasma, where neutrons are mainly generated by so-called beam-thermal reactions. Understanding of S_n in thermal plasma is important in anticipation of establishing steady-state thermal fusion burning plasma. In this study, we surveyed the S_n characteristics in electron cyclotron heated deuterium plasmas in order to show the thermonuclear performance of helical plasma.

2. Experimental Setup

LHD is equipped with five electron cyclotron heating (ECH) systems. Figure 1 (a) shows a schematic drawing of the high-power ECH system and LHD [9]. The ECH launchers are located outside the torus hall, and the power is transferred using waveguides. Three of five electron cyclotron launchers inject a 77 GHz radiofrequency wave corresponding to a fundamental resonance frequency at 2.75 T. The remaining two launchers inject a 154 GHz radiofrequency wave corresponding to a second harmonic resonance frequency at 2.75 T. The total injecting power of the ECH system is up to 5 MW. A neutron flux monitor was used to measure S_n [10, 11]. Figure 1 (b) illustrates the arrangement of the neutron flux monitor. In this experiment, the range order of S_n was less than 10^{12} n/s. Therefore, we employed the low neutron emission rate range system of the neutron flux monitor using a ^{10}B counter installed on the top of LHD. The signal of the ^{10}B counter was fed into the preamplifier (RU156, Toshiba), which was located in the basement of the torus hall. The output signal was

author's e-mail: ogawa.kunihiro@nifs.ac.jp

*) This article is based on the presentation at the 29th International Toki Conference on Plasma and Fusion Research (ITC29).

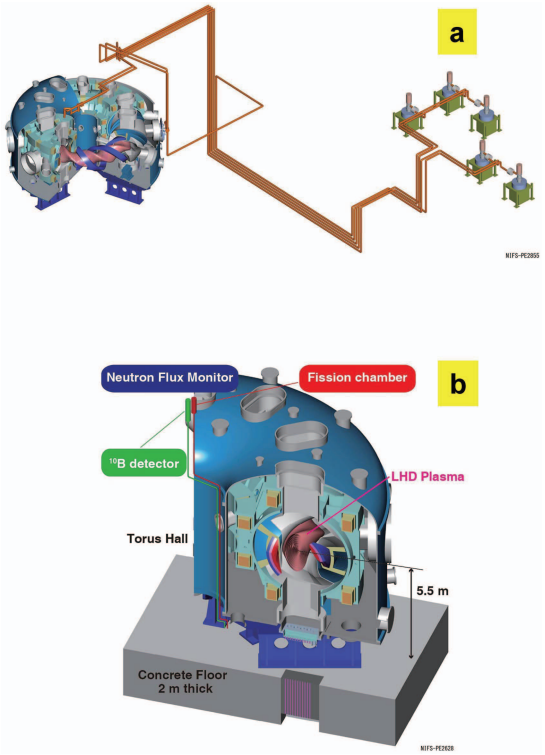

Fig. 1 (a) The ECH system installed on the LHD; (b) the LHD neutron flux monitor.

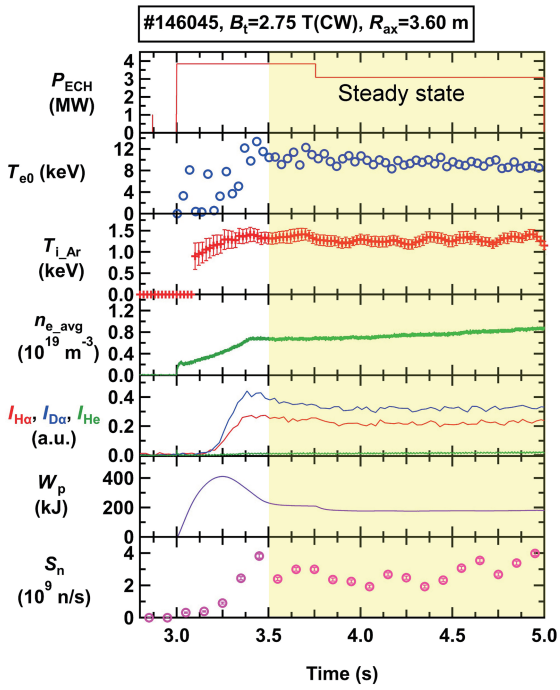

Fig. 2 Typical waveform of the ECH discharge.

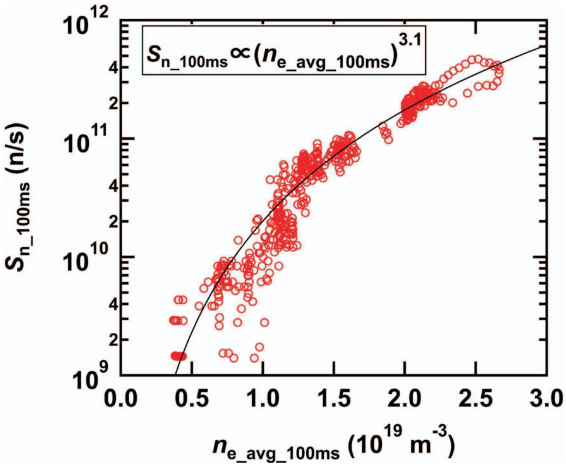

Fig. 3 The electron density dependence of the total neutron emission rate.

sent to the module, having discriminator and electrical-to-optical converter functions (HNB645, Toshiba). The optical signal was transferred from the basement of the torus hall to the diagnostics room and received by the optical-to-electrical convertor (HNB646, Toshiba). The logic pulse from the optical-to-electrical convertor was acquired by the digital counter (PXI-6602, National Instruments). The time bin of the digital counter was set to 1 ms. The line-averaged electron density (n_{e_avg}) was measured using a far-infrared interferometer [12]. Radial profiles of the electron temperature (T_e) and the density (n_e) were measured using Thomson scattering diagnostics [13]. Spectroscopic diagnostics were used to measure argon-ion temperature (T_{i_Ar}), as well as the intensity of Hα line $I_{H\alpha}$, Dα line $I_{D\alpha}$, and He line I_{He} [14].

3. Experimental Results

The typical waveform of the ECH discharge is shown in Fig. 2. In this discharge, toroidal magnetic field strength B_t is 2.75 T, and the preset of magnetic axis position R_{ax} is 3.60 m. When viewed from above, the direction of the toroidal magnetic field is clockwise. Plasma is initiated and sustained by the ECH. The total injection power is 4 MW at the start of the discharge and reduced to 3 MW at a t of 3.75 s. The central electron temperature (T_{e0}) measured by the Thomson scattering diagnostics shows that T_{e0} gradually decreases from 10 keV and n_{e_avg} gradually increases after t of 3.5 s during the discharge. The spectroscopic measurement shows that T_{i_Ar} is close to 1.2 keV. Additionally, the $I_{H\alpha}/I_{D\alpha}$ ratio is almost 2/3 and I_{He} is negligibly low. The plasma-stored energy (W_p) is ~200 - 300 kJ during the discharge. The S_n, measured by the ^{10}B detector of the neutron flux monitor, is $\sim 3 \times 10^9$ n/s. Here the error bar of S_n corresponds to the statistical error of counts. In this analysis, we focused on 3.5 s < t < 5.0 s, where the plasma was nearly in a steady-state condition.

The dependence of S_n on electron density was investigated (Fig. 3). Here, $S_{n\_100\,ms}$ and $n_{e\_avg\_100\,ms}$ represent the 100-ms average values of S_n and n_{e_avg}, respectively. In this plot, $S_{n\_100\,ms}$ is $\sim 10^9$ n/s, where $n_{e\_avg\_100\,ms}$ is $\sim 0.4 \times 10^{19}$ m^{-3}. Then, $S_{n\_100\,ms}$ substantially increases with $n_{e\_avg\_100\,ms}$. Finally, $S_{n\_100\,ms}$ reaches

$\sim 5 \times 10^{11}$ n/s, where $n_{e\_avg\_100\,ms}$ is $\sim 2.7 \times 10^{19}$ m^{-3}. Note that the maximum fusion output in this experiment is $S_n \times 7.25$ MeV $\sim$ 0.6 W. The power function fitting of $S_{n\_100\,ms}$ on $n_{e\_avg\_100\,ms}$ shows that $S_{n\_100\,ms}$ increases with a $n_{e\_avg\_100\,ms}$ power of 3.1. Here, S_n can be expressed as

$$S_n = \frac{1}{2}\int_{V_p}(n_D^2\langle\sigma_{DD}v\rangle)dV = \frac{1}{2}\frac{n_D^2}{n_e^2}\int_{V_p}dV(n_e^2\langle\sigma_{DD}v\rangle),$$

where n_D, $\langle\sigma_{DD}v\rangle$, and V_p represent deuteron density, thermal deuterium-deuterium (DD) fusion reactivity, and plasma volume, respectively. The power greater than 2 shows that S_n has a dependence on not only the absolute value of the deuteron density but also the radial profile of the plasma density, as well as the fuel temperature through DD fusion reactivity.

4. Comparison of Total Neutron Emission Rate in the Experiment and Numerical Simulation

To understand S_n characteristics in ECH plasma, a numerical simulation considering thermal DD fusion reactions [15] was performed. The radial profile of deuteron temperature is assumed to be T_{i0} (1-$(r/a)^2$), where r/a represents the normalized minor radius. Here, T_{i_Ar} is assumed to be the temperature at normalized minor radius of 0.5, therefore, the central deuterium temperature T_{i0} is assumed to be 4/3 of T_{i_Ar}. The ratio of the deuteron density on the electron density is assumed to be the same as $I_{D\alpha}/(I_{D\alpha} + I_{H\alpha} + 2I_{He})$. The radial profile of the deuteron density is assumed to be the same as the electron density profile.

The dependence of S_n in the calculation (S_{n_SIM}) on electron density was obtained as shown in Fig. 4. Although S_{n_SIM} greatly increases with plasma density, the power function fitting of S_{n_SIM} on $n_{e\_avg\_100\,ms}$ shows that S_{n_SIM} increases with a $n_{e\_avg\_100\,ms}$ power of 2.1, which is smaller than the power obtained in experiments. This power close to 2 suggests that the increase in S_n is mainly due to the increase in the absolute value of n_D.

The calculated total neutron emission rate (S_{n_SIM}) is compared with the measured S_n (Fig. 5). Although S_{n_SIM} agrees with experiments when $S_{n\_100\,ms}$ is higher than 4×10^{10} n/s, the numerical simulation overestimates S_n in a relatively low $S_{n\_100\,ms}$ region (less than 4×10^{10} n/s) where n_{e_avg} is less than 1×10^{19} m^{-3}. Although effects of hydrogen and helium are included using visible spectroscopy in this calculation, impurities such as carbon and steel are not included. In low-density region, effective charge becomes larger due to the carbon impurities [16]. The increase of effective charge with the decrease of the plasma density may induce the relatively high S_n in this calculation because n_D is overestimated in the calculation.

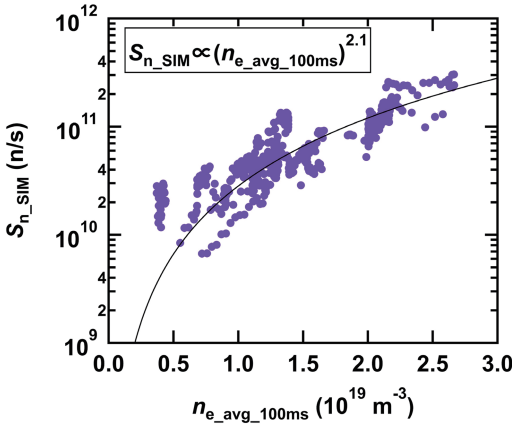

Fig. 4 Calculated total neutron emission rate dependence on the electron density.

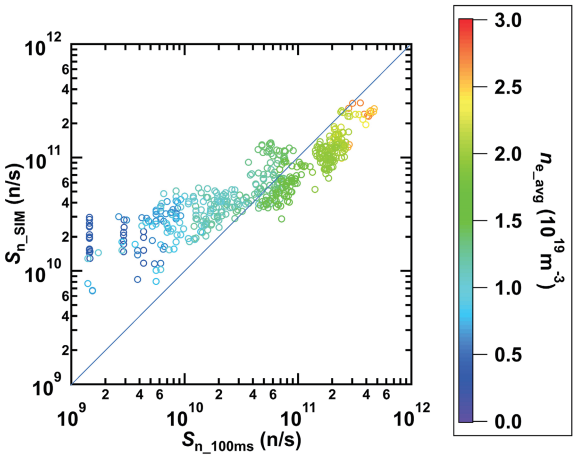

Fig. 5 Comparison of calculated and experimentally obtained S_n. Although calculated S_n agrees with experimental results for a relatively high-density region, they do not match in a relatively low-density region.

5. Summary

The characteristics of S_n in ECH heated LHD plasma were surveyed to highlight the thermonuclear performance of helical plasma. The dependence of S_n on electron density was surveyed with n_{e_avg} from 0.3×10^{19} m^{-3} to 2.7×10^{19} m^{-3}. The experiment showed that S_n increased significantly with an electron density power of 3.1. A numerical simulation based on thermal DD fusion reactions was performed. Although S_n evaluated by the numerical calculations agreed with S_n obtained in the experiment in the relatively high $S_{n\_100\,ms}$ region (corresponding to the high-density region), the numerical calculation overestimated S_n in the relatively low $S_{n\_100\,ms}$ area (corresponding to the low-density region). Changes in the effective charge in relatively low plasma density regions may, thus, be a reason for S_n disagreements in the low $S_{n\_100\,ms}$ region.

Acknowledgments

This work is supported partly by the NIFS Collaboration Research Program (KOAH037), by LHD project budgets (ULGG801, and ULHH034), and by the NINS program of Promoting Research by Networking among Institutions (Grant Number 01411702).

[1] D.L. Jassby *et al.*, Phys. Fluids B **3**, 2308 (1991).
[2] E. Bertolini, Fusion Eng. Des. **27**, 27 (1995).
[3] T. Fujita *et al.*, Nucl. Fusion **39**, 1627 (1999).
[4] Y. Takeiri *et al.*, Nucl. Fusion **57**, 102023 (2017).
[5] Y. Takeiri, IEEE Trans. Plasma Sci. **46**, 2348 (2018).
[6] M. Osakabe *et al.*, IEEE Trans. Plasma Sci. **46**, 2324 (2018).
[7] M. Isobe *et al.*, Nucl. Fusion **58**, 082004 (2018).
[8] K. Ogawa *et al.*, Nucl. Fusion **59**, 076017 (2019).
[9] T. Shimozuma *et al.*, Fusion Sci. Technol. **58**, 530 (2010).
[10] M. Isobe *et al.*, Rev. Sci. Instrum. **85**, 11E114 (2014).
[11] M. Isobe *et al.*, IEEE Trans. Plasma Sci. **46**, 2050 (2018).
[12] T. Akiyama *et al.*, Fusion Sci. Technol. **58**, 352 (2010).
[13] I. Yamada *et al.*, Fusion Sci. Technol. **58**, 345 (2010).
[14] M. Goto *et al.*, Fusion Sci. Technol. **58**, 394 (2010).
[15] R. Seki *et al.*, Plasma Fusion Res. **15**, 1202088 (2020).
[16] X. Huang *et al.*, Plasma Fusion Res. **10**, 3402036 (2015).